Supplementary Information

Competition of quantum anomalous Hall states and charge density wave in a correlated topological model

Xin Gao (高鑫),[1] Jian Sun(孙健),[1] Xiangang Wan(万贤纲), [2,3] and Gang Li(李刚)[1,4,†]

[1]*School of Physical Science and Technology, ShanghaiTech University, Shanghai 201210, China*
[2]*National Laboratory of Solid State Microstructures and School of Physics, Nanjing University, Nanjing 210093, China*
[3]*Collaborative Innovation Center of Advanced Microstructures, Nanjing University, Nanjing 210093, China*
[4]*ShanghaiTech Laboratory for Topological Physics, ShanghaiTech University, Shanghai 201210, China*

I. TIGHT-BINDING MODEL

The tight-binding model studied in this work is a two-orbital model defined on a honeycomb lattice. For simplicity, we only include the nearest-neighbor hopping which couples the two sublattices. On the same sublattice, distinct orbitals are orthogonal. It is easy to show that, under symmetry constrain, $h_{\alpha\alpha}(k) = (3a+b)(1+e^{ik_1})/4+be^{-ik_2}$, $h_{\beta\beta}(k) = (a+3b)(1+e^{ik_1})/4+ae^{-ik_2}$, and $h_{\alpha\beta} = \sqrt{3}(a-b)(1-e^{ik_1})/4$. α, β denote d_{xy} and $d_{x^2-y^2}$, respectively. a, b are model parameters, and k_1, k_2 are the momenta in the first Brillouin zone (BZ), i.e. the fractions of reciprocal lattice vectors $\mathbf{b}_1$ and $\mathbf{b}_2$. On the basis of $|\phi^A_{d_{xy}}\rangle, |\phi^A_{d_{x^2-y^2}}\rangle, |\phi^B_{d_{xy}}\rangle, |\phi^B_{d_{x^2-y^2}}\rangle$, the Hamiltonian matrix can be cast as

$$H_0'(k) = \begin{pmatrix} 0 & 0 & h_{\alpha\alpha}(k) & h_{\alpha\beta}(k) \\ 0 & 0 & h_{\beta\alpha}(k) & h_{\beta\beta}(k) \\ h^*_{\alpha\alpha}(k) & h^*_{\alpha\beta}(k) & 0 & 0 \\ h^*_{\beta\alpha}(k) & h^*_{\beta\beta}(k) & 0 & 0 \end{pmatrix}. \tag{1}$$

As atomic orbitals are orthogonal in the same sublattice, the first and the last 2×2 Hamiltonian blocks are zero. Only the hopping between A-B sublattice contributes. Let us further consider the SOC, it contains both local and nonlocal contributions with the former being the largest term. We neglect the nonlocal SOC, which does not qualitatively affect our model. Atomic SOC between d_{xy} and $d_{x^2-y^2}$ orbitals is a constant. Without it, two eigenvalues of $H_0(k)$ degenerate at K-point at the Fermi level. After including the SOC term, the following Hamiltonian is obtained and a topological gap immediately opens leading to the QAH phase, which is the starting point of our correlated study in this work.

$$H_0(k) = \begin{pmatrix} 0 & 2i\lambda & h_{\alpha\alpha}(k) & h_{\alpha\beta}(k) \\ -2i\lambda & 0 & h_{\beta\alpha}(k) & h_{\beta\beta}(k) \\ h^*_{\alpha\alpha}(k) & h^*_{\alpha\beta}(k) & 0 & 2i\lambda \\ h^*_{\beta\alpha}(k) & h^*_{\beta\beta}(k) & -2i\lambda & 0 \end{pmatrix}. \tag{2}$$

There are three independent parameters a, b, and λ. Depending on the value a/λ and b/λ, there will be three phases with distinct topological numbers, i.e. $c = 0, -1$, and $c = 2$.

The $C = -1$ phase has been shown to correspond exactly to the low-energy excitation of $FeBr_3$ [1]. It is different from Haldane model [2] and Kane-Mele model [3] in the following way: First, our QAH model does not contain any artificial complex hopping term. Instead, a local SOC between the two orbitals triggers the nontrivial topological states of the model. Secondly, our QAH model is a correlated topological model defined for the d_{xy} and $d_{x^2-y^2}$ orbitals, which is a realistic construction for correlated topological systems. Thus, it is interesting to know the effect of electronic correlation on the ground state of this model.

Many previous studies of correlation effect on topological model aim to trigger topological state from Haldane model or Kane-Mele model without the complex hopping term, and expect to generate it from the dynamic evolution. In contrast, we start with a correlated model of intrinsic topology and try to understand its robustness. We characterize the correlated topology by using different approximated methods, as no exact solution is available. We adopt the static mean-field approximation, the dynamical mean-field theory (DMFT), the Cellular DMFT (CDMFT) and exact diagonalization (ED) approaches. These methods are subject to different levels of approximations. By combining them, we expect to reduce numerical bias and obtain a consistent characterization of the correlated topological state. In the following table SI-1, we compare the four approximated approaches in terms of dynamical fluctuations, spatial fluctuations, and thermodynamic limit. A numerically exact method would contain dynamical fluctuation, long-range spatial fluctuations, and is built at thermodynamic limit. By comparing the results from the four approximated methods, we expect to understand the effect of these three features and get insights of the exact solution.

TABLE SI-1. Comparison of the four methods reveals their different levels of approximation.

Method	Dynamical Fluctuations	Spatial Fluctuations	Thermodynamic Limit
Static Mean-Field	No	No	Yes
DMFT	Yes	No	Impurity embedding
CDMFT	Yes	Only short-range	Cluster embedding
ED	Yes	Only short-range	No

A. Chern number

In the tight-binding model and the static mean-field calculations, one obtains the wavefunctions which can be employed to calculate the Chern number from BZ integration. To do this, we follow the recipe of T. Fukui [4] and calculate the Chern number by discretizing BZ into small patches. The Chern number is given by a sum of the winding number of the $U(1)$ gauge transformation along the boundary of a patch. The $U(1)$ link is defined as

$$U_\nu(k_l) \equiv \langle n(k_l)|n(k_l+\hat{\nu})\rangle/\mathcal{N}_\nu(k_l) \ , \tag{3}$$

where ν is a vector denoting direction ν. Along the boundary of a patch, one can define a lattice field strength, whose imaginary part gives rise to the Chern number

$$\tilde{F}_{12}(k_l) \equiv \ln U_1(k_l)U_2(k_l+\hat{1})U_1(k_l+\hat{2})^{-1}U_2(k_l^{-1}) = a + 2\pi i n_{12}(k_l) \ . \tag{4}$$

Here, a is a real number, and the sum of $n_{12}(k_l)$ for all discrete k_l is the Chern number.

$$\text{Chern number} = \sum_l n_{12}(k_l) \ . \tag{5}$$

In our tight-binding and static mean-field calculations, we directly calculate the wave functions and determine the Chern number with 20×20 momentum patches in the first BZ, which is sufficient to get a converged solution. In DMFT, CDMFT, and ED calculations, due to the lack of wave functions and enough momentum resolution, we did not calculate the Chern number.

B. Static mean-field equation

To account for both V_1 and V_2, in the main text, our static mean-field calculations were performed in a six-site unit-cell as shown in Fig. 1**c** of the main text. There are three sites from A-sublattice, and three sites from B-sublattice. d_{xy} and $d_{x^2-y^2}$ orbitals reside at each site. Thus, there are 12 basis functions, which we denote as

$$\{m\}_{1\cdots12} = \{A_1^{d_{xy}}, A_1^{d_{x^2-y^2}}, A_2^{d_{xy}}, A_2^{d_{x^2-y^2}}, A_3^{d_{xy}}, A_3^{d_{x^2-y^2}}, B_1^{d_{xy}}, B_1^{d_{x^2-y^2}}, B_2^{d_{xy}}, B_2^{d_{x^2-y^2}}, B_3^{d_{xy}}, B_3^{d_{x^2-y^2}}\} \ , \tag{6}$$

Tight-binding model expressed at this basis function is a 12×12 matrix. To transform the interaction part to a quadratic form, we further decompose the density-density interaction by the standard mean-field decoupling

$$\hat{n}_{A_i}\hat{n}_{B_j} \approx \langle n_{A_i}\rangle\hat{n}_{B_j} + \hat{n}_{A_i}\langle n_{B_j}\rangle - \langle n_{A_i}\rangle\langle n_{B_j}\rangle \ , \tag{7a}$$

$$\hat{n}_{A_i}\hat{n}_{A_j} \approx \langle n_{A_i}\rangle\hat{n}_{A_j} + \hat{n}_{A_i}\langle n_{A_j}\rangle - \langle n_{A_i}\rangle\langle n_{A_j}\rangle \ . \tag{7b}$$

The mean-field Hamiltonian is simply obtained by appending each diagonal term of the 12×12 tight-binding matrix with a constant dependent on the charge density of the other sites. This term can be generally written as

$$H_{A_\alpha} = V_1\langle n_B\rangle + 3V_2(\langle n_A\rangle - \langle n_{A_i}\rangle) \ , \tag{8a}$$

$$H_{B_\alpha} = V_1\langle n_A\rangle + 3V_2(\langle n_B\rangle - \langle n_{B_i}\rangle) \ . \tag{8b}$$

$\langle n_{A/B}\rangle = \sum_{i=1}^{3}\sum_{\alpha=d_{xy},d_{x^2-y^2}} n_{A_i/B_i,\alpha}$. As each diagonal term differs slightly depending on the charge densities, diagonalizing the new Hamiltonian matrix yields a new set of dispersions $\epsilon_j(k)$ and eigenstates $|\psi_{j,m}(k)\rangle$, where j denotes the j-th eigenstate, and $m \in [1, 12]$ denotes the $m-$th basis component. We proceed to calculate the local density of states $\rho(\epsilon)$ and the new chemical potential μ from

$$\rho(\epsilon) = \frac{1}{N}\sum_{k,j}\delta[\epsilon - \epsilon_j(k)] \ , \int_{-\infty}^{\infty} d\epsilon \frac{\rho(\epsilon)}{\exp[\beta(\epsilon-\mu)+1]} = n_{tot} \ . \tag{9}$$

We fix the particle density to be one per site ($n_{tot} = 6$), corresponding to a half-filling condition, and inverse temperature is taken as $\beta = 1000$. The calculation of new charge density close the mean-field self-consistent loop as

$$\langle n_m \rangle = \frac{1}{N} \sum_k \sum_{j=1}^{12} \frac{|\psi_{j,m}(k)|^2}{\exp[\beta(\epsilon_j(k) - \mu) + 1]} \ . \tag{10}$$

After convergence, we further determine the free energy. Whenever multiple CDW phases are found to be stable in the calculation, we compare their free energy to determine the ground state.

$$\begin{aligned} F = & \frac{1}{N} \sum_k \sum_{j=1}^{12} \frac{\epsilon_k}{\exp[\beta(\epsilon_j(k) - \mu) + 1]} - V_1 \langle n_A \rangle \langle n_B \rangle - 3V_2 (n_{A_1} n_{A_2} + n_{A_1} n_{A_3} + n_{A_2} n_{A_3} + n_{B_1} n_{B_2} + n_{B_1} n_{B_3} + n_{B_2} n_{B_3}) \\ & + k_B T \int d\epsilon \rho(\epsilon) \{ f(\epsilon) \ln[f(\epsilon)] + [1 - f(\epsilon)] \ln[1 - f(\epsilon)] \} \end{aligned} \tag{11}$$

Our self-consistent mean-field calculation starts with a trivial charge density belonging to one of the four states, i.e. 222000, 210210, 220200, and 111111 states. Convergence is achieved if the total difference of the new and old charge density $\Delta = \sum_{m=1}^{12} |\langle n_m^{new} \rangle - \langle n_m^{old} \rangle|$ is smaller than 10^{-5}.

The emergence of the CDW order breaks the symmetry between the two sublattices. Thus, the transition between the QAH phase and the CDW phase does not necessarily close the gap. In the following, we give an intuitive explanation on this point. Following the decomposition of Eq. (7), we update the Hamiltonian Eq. (1) with the correlation effect in the mean-field level and assume there is no orbital order between d_{xy} and $d_{x^2-y^2}$.

$$H^{HF}(k) = \begin{pmatrix} 3V_1 n_B/2 - \mu & 2i\lambda & h_{\alpha\alpha}(k) & h_{\alpha\beta}(k) \\ -2i\lambda & 3V_1 n_B/2 - \mu & h_{\beta\alpha}(k) & h_{\beta\beta}(k) \\ h^*_{\alpha\alpha}(k) & h^*_{\alpha\beta}(k) & 3V_1 n_A/2 - \mu & 2i\lambda \\ h^*_{\beta\alpha}(k) & h^*_{\beta\beta}(k) & -2i\lambda & 3V_1 n_A/2 - \mu \end{pmatrix}. \tag{12}$$

Before the CDW establishes, $n_A = n_B$. The electronic repulsions V_1 only introduce a constant energy term to all bands, which corresponds to a shift of the chemical potential $\mu = 3V_1(n_A + n_B)/2$. Consequently, the charge gap remains the same as the one in the non-interacting limit. When the CDW starts to establish, it creates an energy difference between the A-B sublattice.

$$H^{HF}(k) = \begin{pmatrix} m & 2i\lambda & h_{\alpha\alpha}(k) & h_{\alpha\beta}(k) \\ -2i\lambda & m & h_{\beta\alpha}(k) & h_{\beta\beta}(k) \\ h^*_{\alpha\alpha}(k) & h^*_{\alpha\beta}(k) & -m & 2i\lambda \\ h^*_{\beta\alpha}(k) & h^*_{\beta\beta}(k) & -2i\lambda & -m \end{pmatrix}. \tag{13}$$

Unlike the case of the single-band model where the CDW order parameter always increases the gap, in a multiorbital system, it can either shrink or enlarge the charge gap depending on the amplitude of m, as one will see after diagonalizing Eq. (13). Because m further depends on the charge imbalance of the two sublattices, it is in fact not a free parameter but has to be self-consistently determined. Consequently, the charge gap in a multiorbital model generally does not monotonically change with the increase of the CDW order parameter. Only when m is large enough, does the corresponding free energy become smaller than that of the charge uniform phase, the topological phase transition between the QAH and the CDW occurs with a sudden increase of the CDW order parameter. As shown in Fig.3 of the main text, the first-order phase transition is observed in all calculations. The transition, thus, does not necessarily accompany a gap closure. In Fig. S1, we show the density of states (DOS) from ED calculations on a six-site cluster with periodic boundary conditions. The eight major peaks in each plot correspond to the top and bottom edges of the four bands, thus, the charge gap is easily seen from the peak separation around the Fermi level. In all three topological phase transitions, the charge gap does close and reopen.

II. DYNAMICAL MEAN FIELD THEORY

DMFT is an embedding approach, where a finite-size system called impurity is embedded in the infinite-large lattice. The embedding procedure, on one hand, simplifies the calculations by replacing the problem of solving a lattice Hamiltonian to solving an impurity one. On the other hand, the embedding procedure provides the impurity system a dynamically fluctuating external field, to which the impurity electrons couple. This dynamically fluctuating field is named a hybridization function, which characterizes the coupling between the impurity and the rest of the lattice system. Although the construction of DMFT is conceptually in the thermodynamic limit, the nature of the DMFT approximation respects only the local charge fluctuations.

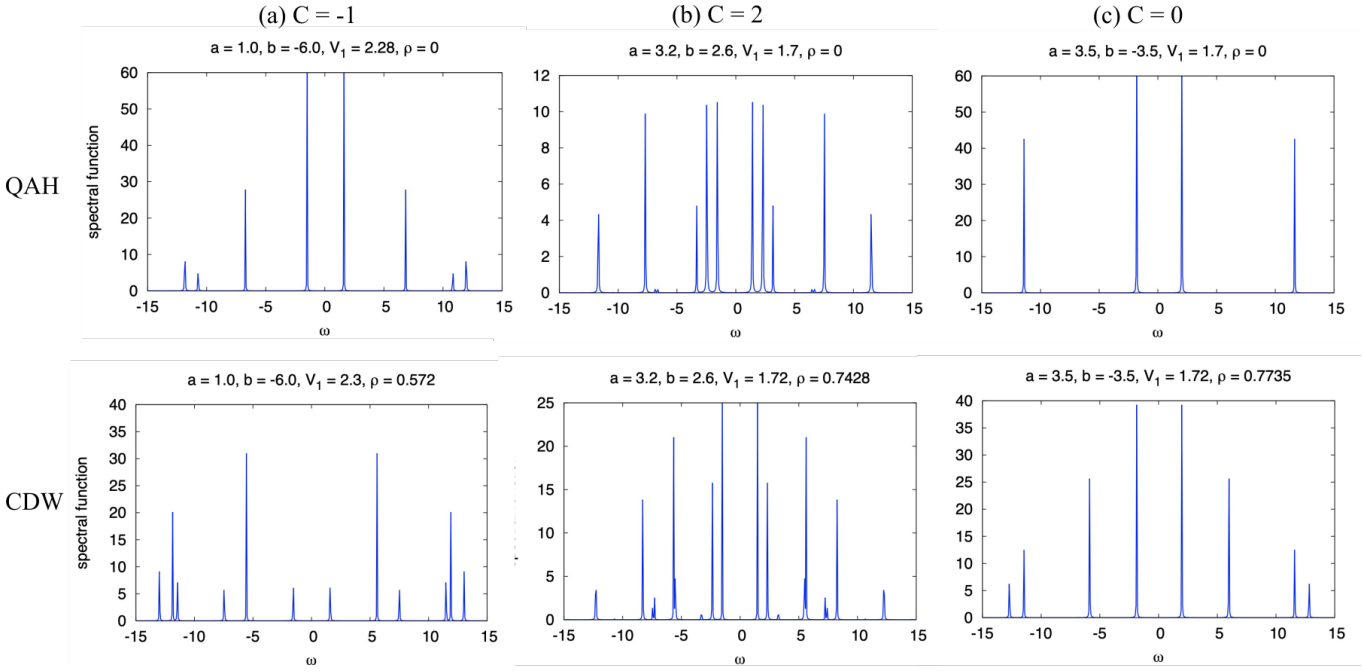

FIG. SI-1. The local DOS before and after the topological phase transition between the QAH and CDW states for all three topological distinct phases. The first row shows the DOS for the QAH phase close to the transition boundary. The second row shows the DOS for the CDW phase slightly after the phase transition. The transition induces an abrupt increase of the CDW order parameter, which is denoted here as ρ. The Fermi level in each plot has been shifted to zero. The charge gap is simply the energy difference between the first two peaks around the Fermi level.

DMFT assumes Green's function of the impurity system to be equal to the local part of the lattice Green's function, which establishes a self-consistent procedure.

$$G^{imp}_{m,n} = \frac{1}{N_k}\sum_k \left[\frac{1}{(i\omega_n+\mu)\mathcal{I} - [H_0(k)] - [\Sigma(i\omega_n)]}\right]_{m,n} , \tag{14}$$

where $\mathcal{I}$ is an unity matrix of the same size of the impurity dimension. In our DMFT study, we take the primitive cell of the honeycomb lattice, which contains two inequivalent sites, as the impurity. $\mathcal{I}$ is then a 4×4 unity matrix. $[H_0(k)]$ is the tight-binding matrix given in Eq. (1), and $[\Sigma(i\omega_n)]$ is the impurity self-energy with the same dimension of the impurity problem. We used ED to solve the impurity problem and obtain $[\Sigma(i\omega_n)]$.

We note that ED works only with Hamiltonians. While, the DMFT embedding procedure spoils the Hamiltonian form of the impurity by introducing the hybridization function, which imposes additional complexity to ED, i.e. the hybridization function needs to be simulated by additional degrees of freedom. For this reason, in ED we work with an Anderson impurity model (AIM), which has the following Hamiltonian form

$$H^{AIM} = \sum_m^{N_d} \epsilon_m d^\dagger_m d_m + \sum_l^{N_{bath}} \epsilon_l a^\dagger_l a_l + \sum_l (W_{lm} a^\dagger_l d_m + h.c.) + V_1 \sum_{m_1 m_2} n_{m_1} n_{m_2} . \tag{15}$$

$d^\dagger_m(d_m)$ is the creation (annihilation) operator of the impurity electron, and $N_d = 4$. V_1 is the Coulomb interaction between neighboring sites. ϵ_m is the impurity energy level. ϵ_l and W_{lm} are additional parameters introduced to simulate the hybridization function. They are often called bath degrees of freedom. In our calculation, we take $N_{bath} = 8$ and a shared-bath topology.

$$[G^{imp,-1}(i\omega_n) + \Sigma(i\omega_n)] = [i\omega_n + \mu - E_{loc} - \sum_l \frac{W^*_{m_1 l} W_{l m_2}}{i\omega_n - \epsilon_l}] , \tag{16}$$

where E_{loc} is the impurity energy level and corresponds to the local part of Eq. (1). We use χ^2-minimization to fit the left side of the above equation by choosing appropriate W_{lm} and ϵ_l. The quality of the DMFT solution, therefore, depends on the quality of fitting. In our calculations, we always carefully check the fitting parameters and, most of the time, we use the converged fitting values of $\{W, \epsilon\}$ at the neighboring parameters $a/\lambda, b/\lambda, V_1/\lambda, V_2/\lambda$ as initial values. For the DMFT calculations, we directly

used the lapack routine to diagonalize the Anderson impurity Hamiltonian. While, for the six-site CDMFT equations, we used the Lanczos algorithm [5] and also includes the nest nearest-neighbor interaction V_2.

We briefly summarize the advantages and limitations of our DMFT calculation. Understanding the condition of applicability is essential for interpreting the results and summarizing the general conclusions independent of any specific method. (1). Compared to the static mean-field theory presented in the previous section, DMFT contains dynamic fluctuations which will influence both the QAH and the CDW states. (2). The local approximation of DMFT allows only local charge fluctuations to be considered. (3). ED only works with Hamiltonian form, such that we have to use additional bath degrees of freedom to simulate the hybridization function. Limited by the memory size, one cannot take as many bath sites as wanted. In our calculations, we take $N_{bath} = 8$, which we found sufficient to fit the hybridization function with good accuracy. (4). A better treatment of non-local Coulomb interaction requires an extended-DMFT calculation, in which interactions become dynamical. Here, we simply truncate the interaction beyond the impurity size, which results in a simplification. From such approximation, we underestimate the effect of V_1 and V_2. Thus, the results we obtained provide an upper bound of the phase boundary between QAH and CDW.

[1] Q. Sui, J. Zhang, S. Jin, Y. Xia, and G. Li, Chinese Physics Letters **37**, 097301 (2020).
[2] F. D. M. Haldane, Phys. Rev. Lett. **61**, 2015 (1988).
[3] C. L. Kane and E. J. Mele, Phys. Rev. Lett. **95**, 146802 (2005).
[4] T. Fukui, Y. Hatsugai, and H. Suzuki, Journal of the Physical Society of Japan **74**, 1674 (2005).
[5] C. Lanczos, J. Res. Natl. Bur. Stand. B **45**, 255 (1950).